Product Rotational Polarization in Photo-initiated Bimolecular Reactions A+BC: Dependence on the Character of the Potential Energy Surface for Different Mass Combinations

Ming-Liang Wang, Ke-Li Han,* and Guo-Zhong He

State Key Laboratory of Molecular Reaction Dynamics, Dalian Institute of Chemical Physics, Chinese Academy of Sciences, Dalian 116023, China

Received: April 3, 1998; In Final Form: September 23, 1998

In cases of light−heavy−light (LHL), light−light−heavy (LLH), and light−heavy−heavy (LHH) mass combinations, the product rotational polarization is reported using the quasiclassical trajectory method in the photoinitiated bimolecular reaction A + BC → AB + C on attractive, mixed, and repulsive surfaces. Four polarization-dependent differential cross sections (PDDCS) which are sensitive to many photoinitiated bimolecular reaction experiments are presented. Furthermore, the dihedral angle distribution $P(\phi_r)$ characterizing the **K**−**K′**−**J′** correlation and the distribution of angle between **K** and **J′** $P(\theta_r)$ are discussed. Finally, the angular distributions $P(\theta_r,\phi_r)$ of product rotational vectors in the form of polar plots in θ_r and ϕ_r are shown.

I. Introduction

Chemical reactions have been studied mainly by the measurements and calculations of scalar properties such as rate constant, cross section, product population distributions, etc. However, vector correlations[1] represent an interesting probe to understand the stereodynamics underlying chemical reactions. Fano, Herschbach, and co-workers have undertaken some pioneering works on dynamical sterochemistry.[2−5] Vector properties, such as velocities and angular momentum, possess not only magnitudes that can be directly related to translational and rotational energies but also well defined directions. Only by understanding the scalar and vector properties together can the fullest picture of the scattering dynamics emerge. The correlations of three vectors, **K, K′** (the reagent and product relative velocity vectors), and **J′** (the product rotational angular momentum) in the CM frame can be characterized by some interesting double and triple vector correlations.[6]

Many past experiments have determined the product rotational polarization using polarization-resolved chemiluminescence, polarized laser-induced fluorescence, electric deflection methods, etc., under molecular-beam and bulb conditions.[7−13] Over the last 3 decades, these methods have become standard. In the past few years, with the development of Doppler-resolved or time-of-flight strategies used in probing the product state selective dynamics of photo-initiated bimolecular reactions, the product polarization has been measured.[14−16] Recently, many studies have yielded product state selective rotational polarization.[17−21]

In order to rationalize experimental results, the assistance of computational work is necessary. Up until now, only limited theoretical calculations, using quasiclassical trajectory methods, quantum-scattering or wave packet propagation techniques,[6,22−27] have been concerned with vector correlations, perhaps because of a shortage of experimental data with which to make comparisons. One should note that Hijazi and Polanyi have used QCT methods on two potential energy surfaces, one attractive and one repulsive, to investigate the effects of different mass combinations on the distribution of angles between product rotational angular momentum and reagent relative velocity and the role of reagent orbital angular momentum in determining **J′**.[23,24] Moreover, the effect of the energy barrier location on the product alignment at different collision energies has been studied by Han and co-workers.[25] For photon-initiated bimolecular reactions, a unified, semiclassical treatment of the center-of-mass correlated (**K, K′, J′**) angular distribution recently has been described recently by Aoiz et al.,[6] where the strategy developed is well suited to the theoretical calculation of product polarization, in particular, using quasiclassical trajectory methods. In a previous paper, for heavy−heavy−light (HHL), heavy−light−light (HLL), heavy−light−heavy (HLH), and heavy−heavy−heavy (HHH) or light−light−light (LLL) mass combinations, the product polarization on attractive, mixed, and repulsive surfaces have been discussed.[36]

II. Theory

A. Product Rotational Polarization. The CM (center-of-mass) frame is chosen, whose *z*-axis lies in the direction of the reagent relative velocity **K** and the *y* axis is perpendicular to the *xz* plane containing **K** and **K′**.[6] The fully correlated center-of-mass angular distribution is written as the sum[6,28,34]

$$P(\omega_t,\omega_r) = \sum_{kq} \frac{[k]}{4\pi} \frac{1}{\sigma} \frac{d\sigma_{kq}}{d\omega_t} C_{kq}(\theta_r,\phi_r)^* \qquad (1)$$

where $[k] = 2k + 1$, $(1/\sigma)(d\sigma_{kq}/d\omega_t)$ is a generalized polarization-dependent differential cross section (PDDCS),[6] $C_{kq}(\theta_r\phi_r)$ are modified spherical harmonics,[28] and $1/\sigma\ d\sigma_{kq}/d\omega_t$ yields[34]

$$1/\sigma\ d\sigma_{k0}/d\omega_t = 0 \qquad k \text{ is odd}$$

$$1/\sigma\ d\sigma_{kq+}/d\omega_t = 1/\sigma\ d\sigma_{kq}/d\omega_t + 1/\sigma\ d\sigma_{k-q}/d\omega_t = 0$$
$$k \text{ is even}, \quad q \text{ is odd or } k \text{ is odd}, \quad q \text{ is even}$$

* Author to whom all correspondence should be addressed.

10.1021/jp981738u CCC: $15.00
Published on Web 11/24/1998

$$\frac{1}{\sigma}\frac{d\sigma_{kq-}}{d\omega_t} = \frac{1}{\sigma}\frac{d\sigma_{kq}}{d\omega_t} - \frac{1}{\sigma}\frac{d\sigma_{k-q}}{d\omega_t} = 0$$

k is even, q is even or k is odd, q is odd

The PDDCS is written as follows:

$$\frac{1}{\sigma}\frac{d\sigma_{kq\pm}}{d\omega_t} = \sum_{k_1}\frac{[k_1]}{4\pi} S^{k_1}_{kq\pm}\, C_{k_1-q}(\theta_t,0) \tag{2}$$

where the $S^{k_1}_{q\pm}$ are evaluated using the expected expression:

$$S^{k_1}{}_{kq\pm} = \langle c_{k_1 q}(\theta_t,0) c_{kq}(\theta_r,0)[(-1)^q e^{iq\phi_r} \pm e^{-iq\phi_r}]\rangle \tag{3}$$

where the angular brackets represent an average over all angles.

The differential cross-section is given by

$$\frac{1}{\sigma}\frac{d\sigma_{00}}{d\omega_t} \equiv P(\omega_t) = \frac{1}{4\pi}\sum_{k_1}[k_1] h^{k_1}_0(k_1,0) P_{k_1}(\cos\theta_t) \tag{4}$$

The bipolar moments $h^{k_1}_0(k_1,0)$ are evaluated using the expected expression,

$$h^{k_1}_0(k_1,0) = \langle P_{k_1}(\cos\theta_t)\rangle \tag{5}$$

The PDDCS with $q = 0$ is presented by

$$\frac{1}{\sigma}\frac{d\sigma_{k0}}{d\omega_t} = \frac{1}{4\pi}\sum_{k_1}[k_1] S^{k_1}_{k0} P_{k_1}(\cos\theta_t) \tag{6}$$

where $S^{k_1}_{k0}$ are evaluated by the expected expression

$$S^{k_1}_{k0} = \langle P_{k_1}(\cos\theta_t) P_k(\cos\theta_r)\rangle \tag{7}$$

As shown in refs 28 and 30, many photoinitiated bimolecular reaction experiments will be sensitive to only those polarization moments with $k = 0$ and $k = 2$. In order to compare calculations with experiments, $(2\pi/\sigma)(d\sigma_{00}/d\omega_t)$, $(2\pi/\sigma)(d\sigma_{20}/d\omega_t)$, $(2\pi/\sigma)(d\sigma_{22+}/d\omega_t)$, and $(2\pi/\sigma)(d\sigma_{21-}/d\omega_t)$ are calculated.

The usual two vector correlation ($\mathbf{K}-\mathbf{J}'$) is expanded in a series of Legendre polynomials, and the distribution $P(\theta_r)$ can be written[6,28,29]

$$P(\theta_r) = {}^1/_2 \sum_k [k] a^k_0 P_k(\cos\theta_r) \tag{8}$$

The a^k_0 coefficients (polarization parameters) are given by

$$a^k_0 = \langle P_k(\cos\theta_r)\rangle \tag{9}$$

where the angular brackets represent an average over all the reactive trajectories.

The dihedral angle distributions of the $\mathbf{K}-\mathbf{K}'-\mathbf{J}'$, $\mathbf{K}-\mathbf{K}'-\mathbf{L}$ ($\mathbf{L}$ is the reagent orbital angular momentum), and $\mathbf{K}-\mathbf{K}'-\mathbf{L}'$ ($\mathbf{L}'$ is the product orbital angular momentum) three vector correlation are characterized by the angle ϕ_r, ϕ_L, and $\phi_{L'}$, respectively.[6,28] It has been shown that the distribution of the dihedral angle ϕ_r could be expanded as a Fourier series. The ϕ_r distribution can be written as

$$P(\phi_r) = \frac{1}{2\pi}(1 + \sum_{n\ \text{even}\ \geq 2} a_n \cos n\phi_r + \sum_{n\ \text{odd}\geq 1} b_n \sin n\phi_r) \tag{10}$$

with a_n and b_n given by

$$a_n = 2\langle \cos n\phi\rangle \tag{11}$$

The joint probability density function of angles θ_r and ϕ_r,

$$b_n = 2\langle \sin n\phi_r\rangle \tag{12}$$

which define the direction of $\mathbf{J}'$, can be written as[6,30]

$$P(\theta_r,\phi_r) = \frac{1}{4\pi}\sum_{kq}[k] a^k_q C_{kq}(\theta_r,\phi_r)^* = \frac{1}{4\pi}\sum_k\sum_{q\geq 0}[a^k_{q\pm}\cos q\phi_r - a^k_{q\mp} i \sin q\phi_r] C_{kq}(\theta_r,0) \tag{13}$$

In the calculation, the polarization parameter a^k_q is evaluated as

$$a^k_{q\pm} = 2\langle C_{k|q|}(\theta_r,0)\cos q\phi_r\rangle \qquad k\ even \tag{14}$$

$$a^k_{q\pm} = 2i\langle C_{k|q|}(\theta_r,0)\sin q\phi_r\rangle \qquad k\ \text{odd} \tag{15}$$

B. Quasiclassical Trajectory Calculations. The classical Hamilton's equations are integrated numerically for motion in three dimensions.[31] The trajectory is initiated with the BC molecule in the $v = 0$ and $j = 0$ levels, and the collision energy is 10.0 kcal/mol. In our calculations, 20000 trajectories are sampled, and the statistical uncertainty is less than 1.5%. The mass of L and H are 1 and 80 amu, respectively.

C. Potential Energy Surface. The extended LEPS potential energy surface which favors the collinear approach is employed in these calculations[25,32,35]

$$V(r_1,r_2,r_3) = Q_1 + Q_2 + Q_3 - (J_1^2 + J_2^2 + J_3^2 - J_1J_2 - J_1J_3 - J_2J_3)^{1/2} \tag{16}$$

where

$$Q_i = ({}^1E_i + {}^3E_i)/2 \tag{17}$$

$$J_i = ({}^1E_i - {}^3E_i)/2 \tag{18}$$

${}^1E_i$ is defined as the diatomic Morse potential function, and ${}^3E_i$ stands for the anti-Morse function,

$${}^1E_i = D_i(\{1 - \exp[-\beta_i(r - r_0)]\}^2 - 1) \tag{19}$$

$${}^3E_i = {}^3D_i(\{1 + \exp[-\beta_i(r - r_0)]\}^2 - 1) \tag{20}$$

where

$${}^3D_i = D_i(1 - S_i)/2(1 + S_i) \tag{21}$$

and S_i is an adjustable parameter. Subscript $i = 1$, 2, and 3 indicates AB, BC, and AC, respectively. The parameters of attractive, mixed and repulsive potential energy surfaces, taken from ref 33, are listed in Table 1. The contours of the three potential energy surfaces are given in Figure 1. As discussed in ref 33, on surface a, 72% of energy release is attractive energy. In case of surface c, 97% of energy release is repulsive

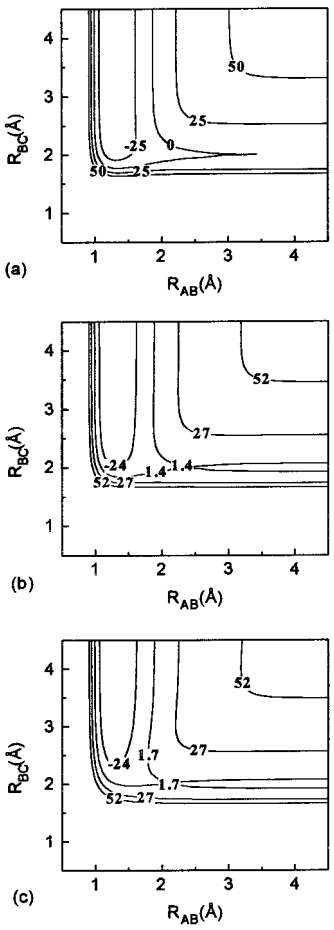

Figure 1. Potential energy surfaces for collinear reaction A + BC → AB + C. (a) Attractive potential energy surface. (b) Mixed potential energy surface. (c) Repulsive potential energy surface.

TABLE 1: Parameters of Potential Energy Surfaces for A + BC

PES	species	D_e(kcal/mol)	β (Å^{-1})	r_0(Å)	S_i
repulsive	AB	106.4	1.87	1.27	0.1
	BC	57.9	2.02	1.99	−0.25
	AC	106.4	1.87	1.27	0.1
mixed	AB	106.4	1.87	1.27	0.05
	BC	57.9	4.04	1.99	0.05
	AC	106.4	1.87	1.27	0.05
attractive	AB	106.4	1.87	1.27	0.20
	BC	57.9	2.02	1.99	0.20
	AC	106.4	1.87	1.27	0.20

energy. However, on surface b, 47% of energy release is attractive energy, and 53% of energy release is repulsive energy.

Results and Discussions

In the computation, the expansions of $P(\theta_r)$, $P(\phi_r)$, PDDCS and $P(\theta_r,\phi_r)$ have been truncated. Except for the results in Figure 2, $P(\phi)$ is expanded up to $n = 24$, the distribution of $P(\theta_r)$ is obtained employing Legendre moments with $k = 18$, and PDDCSs are expanded up to $k_1 = 7$, the plot of $P(\theta_r,\phi_r)$ is calculated using the expansion given in eq 13 with $k = 7$. As the expansions have been truncated, it is necessary to check the convergence of the calculated results. In Figure 2, the product rotational polarization are calculated again for the LHL mass combination on attractive surface, where $P(\theta_r)$, $P(\phi_r)$, PDDCS, and $P(\theta_r,\phi_r)$ $P(\theta_r)$ are expanded up to $k = 14$, $n = 20$, $k_1 = 6$, and $k = 6$, respectively. By comparing the results in Figures 2 and 3, it is concluded that the calculated results in Figure 3 show good convergence.

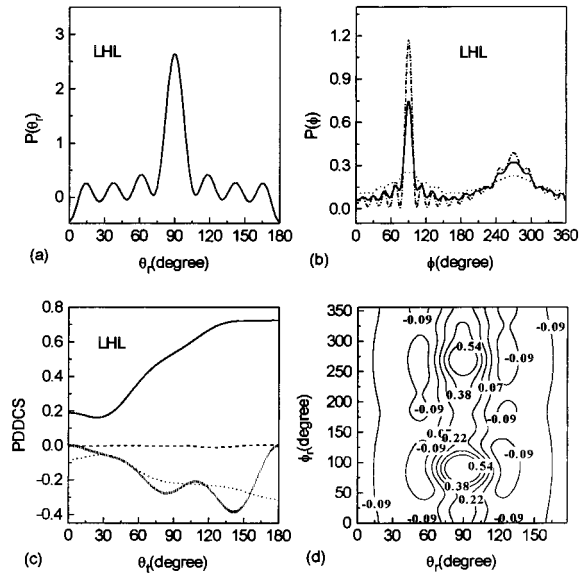

Figure 2. The results on attractive surface for the LHL mass combination. (a) The distribution of $P(\theta_r)$, reflecting the **K**−**J**′ correlation. (b) Solid line indicating the distribution $P(\phi_r)$, dotted line indicating $P(\phi_{L'})$, dot−dashed line indicating $P(\phi_L)$. (c) Four PDDCSs, solid line indicating $(2\pi/\sigma)(d\sigma_{00}/d\omega)$, dot-line indicating $(2\pi/\sigma)(d\sigma_{20}/d\omega)$, short vertical line indicating $(2\pi/\sigma)(d\sigma_{22+}/d\omega)$, and short dashed line indicating $(2\pi/\sigma)(d\sigma_{21-}/d\omega)$. (d) Polar plots of $P(\theta_r,\phi_r)$ distribution averaged over all scattering angles.

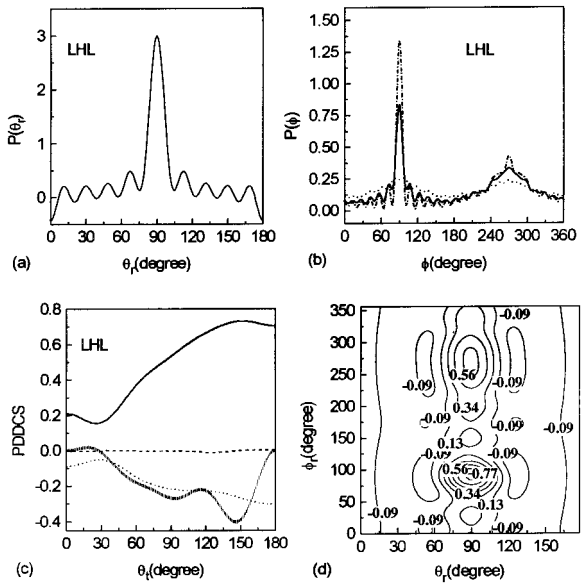

Figure 3. The results on attractive surface for the LHL mass combination. (a) The distribution of $P(\theta_r)$, reflecting the **K**−**J**′ correlation. (b) Solid line indicating the distribution $P(\phi_r)$, dotted line indicating $P(\phi_{L'})$, dot−dashed line indicating $P(\phi_L)$. (c) Four PDDCSs, solid line indicating $(2\pi/\sigma)(d\sigma_{00}/d\omega)$, dotted line indicating $(2\pi/\sigma)(d\sigma_{20}/d\omega_t)$, short vertical line indicating $(2\pi/\sigma)(d\sigma_{22+}/d\omega)$ and short dashed line indicating $(2\pi/\sigma)(d\sigma_{21-}/d\omega_t)$. (d) Polar plots of $P(\theta_r,\phi_r)$ distribution averaged over all scattering angles.

A. Light−Heavy−Light (LHL) Mass Combination. The calculated results on the attractive, mixed, and repulsive surfaces are respectively presented in Figures 3 to 5. Following the distribution of $P(\theta_r)$, which represents the **K, J**′ correlation, one can conclude that the product rotational alignment is very strong. By comparing the results of the three surfaces, $P(\theta_r)$ is almost

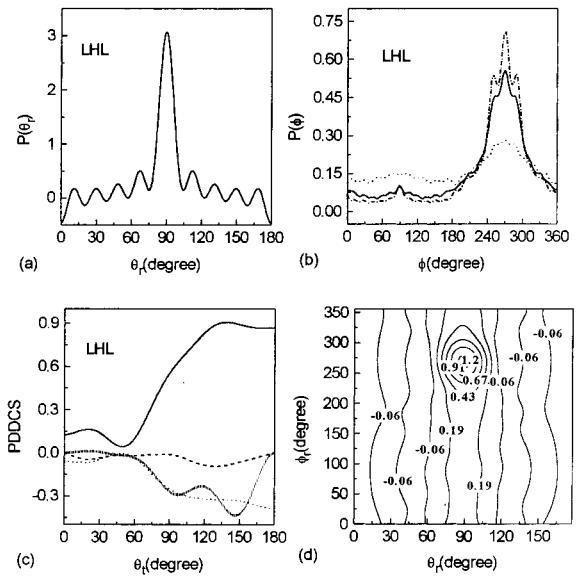

Figure 4. The results on mixed surface for LHL mass combination. (a) The distribution of $P(\theta_r)$, reflecting the $\mathbf{K}-\mathbf{J}'$ correlation. (b) Solid line indicating the distribution $P(\phi_r)$, dotted line indicating $P(\phi_L)$, dot−dashed line indicating $P(\phi_L)$. (c) Four PDDCSs, solid line indicating $(2\pi/\sigma)(d\sigma_{00}/d\omega)$, dotted line indicating $(2\pi/\sigma)(d\sigma_{20}/d\omega)$, short vertical line indicating $(2\pi/\sigma)(d\sigma_{22+}/d\omega)$ and short dashed line indicating $(2\pi/\sigma)(d\sigma_{21-}/d\omega_t)$. (d) Polar plots of $P(\theta_r,\phi_r)$ distribution averaged over all scattering angles.

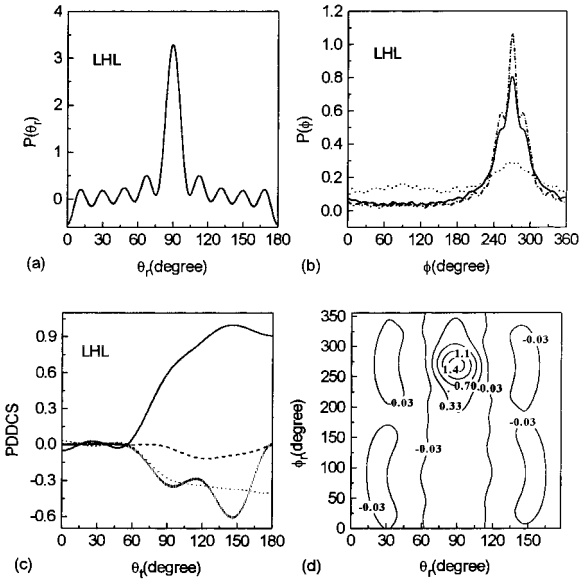

Figure 5. The results on repulsive surface for the LHL mass combination. (a) The distribution of $P(\theta_r)$, reflecting the $\mathbf{K}-\mathbf{J}'$ correlation. (b) Solid line indicating the distribution $P(\phi_r)$, dotted line indicating $P(\phi_{L'})$, dot−dashed line indicating $P(\phi_L)$. (c) Four PDDCSs, solid line indicating $(2\pi/\sigma)(d\sigma_{00}/d\omega_t)$, dotted line indicating $(2\pi/\sigma)(d\sigma_{20}/d\omega_t)$, short vertical line indicating $(2\pi/\sigma)(d\sigma_{22+}/d\omega_t)$ and short dashed line indicating $(2\pi/\sigma)(d\sigma_{21-}/d\omega_t)$. (d) Polar plots of $P(\theta_r,\phi_r)$ distribution averaged over all scattering angles.

independent of the surfaces. According to conservation of angular momentum in the reaction A + BC → AB + C,

$$\mathbf{L} + \mathbf{J} = \mathbf{J}' + \mathbf{L}' = \mathbf{J}_{tot} \tag{22}$$

where $\mathbf{J}_{tot}$ is the total angular momentum in the reaction and $\mathbf{J}$ is the reactant rotational angular momentum. From following the distributions of $P(\theta)$ and the mean value of $\mathbf{L}$, $\mathbf{L}'$ and $\mathbf{J}'$, it is concluded that $\mathbf{J}'$ is approximately equal to $\mathbf{L}$. In this case, the reactant orbital angular momentum $\mathbf{L}$ plays an important role on the distribution of $P(\theta_r)$. One should note that $P(\theta_r)$ is more difficult to converge for the LHL mass combination than other mass combinations. This may result from the fact that the product rotational alignment is strong for the LHL mass combination at a collision energy of 10.0 kcal/mol.

From the dihedral angle distribution of the $\mathbf{K}-\mathbf{K}'-\mathbf{J}'$, one comes to realize that $P(\phi_r)$ tends to be very asymmetric with respect to the scattering plane, directly reflecting the strong polarization of angular momentum induced by the potential energy surface. The asymmetry in the $P(\phi_r)$ distributions reflects the strong orientation. On the attractive surface, a strong peak appears at ϕ_r close to 90°, which is connected with molecular products with counterclockwise rotation. However, on the mixed and repulsive surfaces, the strong peak is shown at ϕ_r close to 270°, which is related to the product molecules with clockwise rotation. As the distributions of $P(\phi_L)$ and $P(\phi_r)$ show similar trends, $P(\phi_r)$ is mainly determined by reactant orbital angular momentum $\mathbf{L}$ for LHL mass combination. On the attractive surface, $\mathbf{J}'$ and $\mathbf{L}$ are parallel to each other. Obviously, the distribution of $P(\phi_r)$ is sensitive to the characteristics of the surfaces.

The PDDCS $(2\pi/\sigma)(d\sigma_{00}/d\omega_t)$ is a simple differential cross-section. On these three potential energy surfaces, the product molecules are scattered backward. The value of PDDCS $(2\pi/\sigma)(d\sigma_{20}/d\omega_t)$ shows a trend which is opposite to that of $(2\pi/\sigma)(d\sigma_{00}/d\omega_t)$, indicating that $\mathbf{J}'$ is strongly aligned perpendicular to $\mathbf{K}$. When the reaction shows a strong product rotational alignment, such a behavior is easily understood from eqs 6 and 7. The PDDCS $(2\pi/\sigma)(d\sigma_{22+}/d\omega_t)$, which provides information on ϕ_r, is very interesting. At the extremes of forward and backward scattering, the PDDCSs with $q \neq 0$ are necessarily zero.[6] At these limiting scattering angles, the $\mathbf{K}-\mathbf{K}'$ scattering plane is not determined and the value of these PDDCSs must be zero. On all three surfaces, $(2\pi/\sigma)(d\sigma_{22+}/d\omega_t)$ strongly depends on the scattering angle. The inspection of $(2\pi/\sigma)(d\sigma_{22+}/d\omega_t)$, which is negative for backward scattering, reveals an noticeable preference for an alignment of $\mathbf{J}'$ along the y axis as opposed to the x axis. The value of PDDCS $(2\pi/\sigma)(d\sigma_{21-}/d\omega_t)$ is close to zero on three surfaces, that is to say, $(2\pi/\sigma)(d\sigma_{21-}/d\omega_t)$ is obviously isotropic and almost independent of surfaces. In one word, $(2\pi/\sigma)(d\sigma_{21-}/d\omega_t)$, $(2\pi/\sigma)(d\sigma_{00}/d\omega_t)$, $(2\pi/\sigma)(d\sigma_{20}/d\omega_t)$, and $(2\pi/\sigma)(d\sigma_{22+}/d\omega_t)$ are weakly influenced by surfaces for LHL mass combination. From the distribution of $P(\theta_r,\phi_r)$, the strongest peak appears at (90°, 90°) on the attractive surface; however, the strongest peak at (90°, 270°) is presented on mixed and repulsive surfaces. It is in good accordance with the distributions of $P(\theta_r)$ and $P(\phi_r)$.

B. Light−Light−Heavy (LLH) Mass Combination. Figures 6−8 show the plots of $P(\theta_r)$, $P(\phi_r)$, four PDDCSs, and $P(\theta_r,\phi_r)$ for LLH mass combination on attractive, mixed and repulsive surfaces, respectively. Clearly, $P(\theta_r)$ is strongly affected by the type of surface. Upon comparing the results with that of the LHL mass combination, one finds that the distribution of $P(\theta_r)$ is sensitive to two factors at the same collision energy, one is character the of surfaces, the other is mass combination. For the LLH mass combination, the surfaces play an important role on $P(\theta_r)$. The distribution of $P(\theta_r)$ becomes more broad with the repulsive energy increment. In the case of the LLH mass combination, $\mathbf{L}'$ is large, and the repulsive energy plays an important role on $P(\theta_r)$.

From the distribution of $P(\phi_r)$, it is found that the number of molecular products which are scattered with $\phi_r \leq \pi$ are much

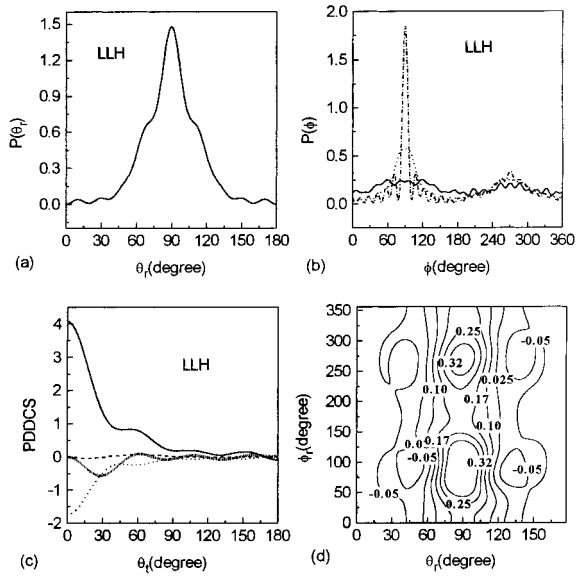

Figure 6. The results on attractive surface for the LLH mass combination. (a) The distribution of $P(\theta_r)$, reflecting the $\mathbf{K}-\mathbf{J}'$ correlation. (b) Solid line indicating the distribution $P(\phi_r)$, dotted line indicating $P(\phi_{L'})$, dot−dashed line indicating $P(\phi_L)$. (c) Four PDDCSs, solid line indicating $(2\pi/\sigma)(d\sigma_{00}/d\omega_t)$, dotted line indicating $(2\pi/\sigma)$-$(d\sigma_{20}/d\omega_t)$, short vertical line indicating $(2\pi/\sigma)(d\sigma_{22+}/d\omega_t)$, and short dashed line indicating $(2\pi/\sigma)(d\sigma_{21-}/d\omega_t)$. (d) Polar plots of $P(\theta_r,\phi_r)$ distribution averaged over all scattering angles.

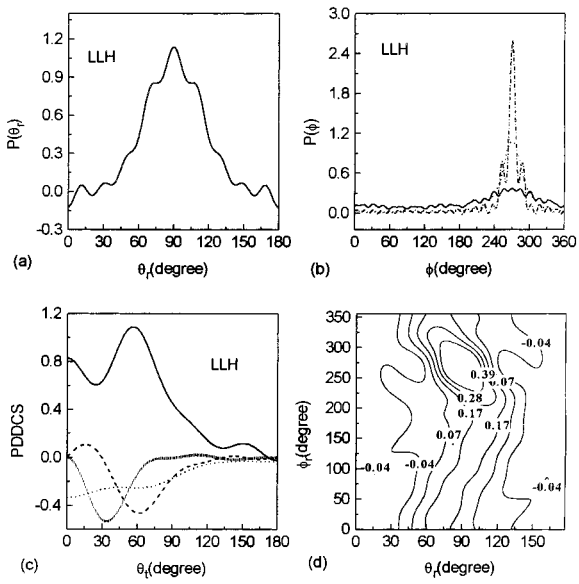

Figure 7. The results on mixed surface for the LLH mass combination. (a) The distribution of $P(\theta_r)$, reflecting the $\mathbf{K}-\mathbf{J}'$ correlation. (b) Solid line indicating the distribution $P(\phi_r)$, dotted line indicating $P(\phi_{L'})$, dot−dashed line indicating $P(\phi_L)$. (c) Four PDDCSs, solid line indicating $(2\pi/\sigma)(d\sigma_{00}/d\omega_t)$, dotted line indicating $(2\pi/\sigma)(d\sigma_{20}/d\omega)$, short vertical line indicating $(2\pi/\sigma)(d\sigma_{22+}/d\omega_t)$ and short dashed line indicating $(2\pi/\sigma)(d\sigma_{21-}/d\omega_t)$. (d) Polar plots of $P(\theta_r,\phi_r)$ distribution averaged over all scattering angles.

more than those scattered with $\phi_r \geq \pi$ on the attractive surface. However, on mixed and repulsive surfaces, most of the molecular products are produced with $\phi_r \geq \pi$, which may be explained from the distributions of $P(\phi_{L'})$, $P(\phi_L)$, and $P(\phi_r)$. Following the distributions of $P(\phi_{L'})$, $P(\phi_L)$, and $P(\phi_r)$and their mean value in Table 2, the propensity $\mathbf{L} \rightarrow \mathbf{L}'$ is shown for the LLH mass combination. The distribution of $P(\phi_r)$ appears more broad on all three surfaces than $P(\phi_r)$ of the LHL mass combination. Obviously, $P(\phi_r)$ is sensitive to surface type.

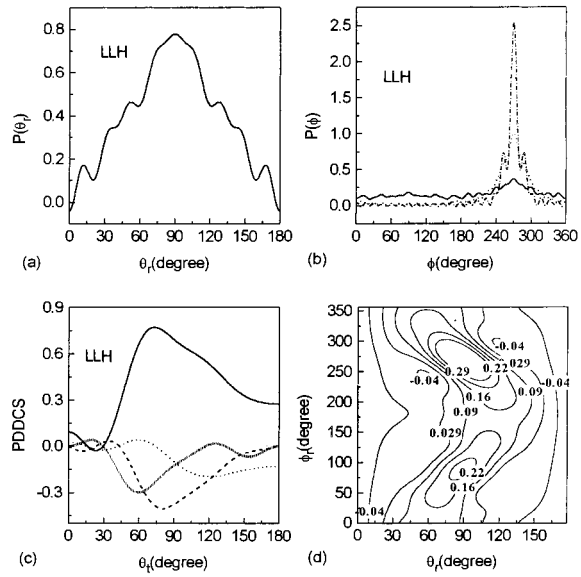

Figure 8. The results on repulsive surface for the LLH mass combination. (a) The distribution of $P(\theta_r)$, reflecting the $\mathbf{K}-\mathbf{J}'$ correlation. (b) Solid line indicating the distribution $P(\phi_r)$, dotted line indicating $P(\phi_{L'})$, dot−dashed line indicating $P(\phi_L)$. (c) Four PDDCSs, solid line indicating $(2\pi/\sigma)(d\sigma_{00}/d\omega_t)$, dotted line indicating $(2\pi/\sigma)$-$(d\sigma_{20}/d\omega_t)$, short vertical line indicating $(2\pi/\sigma)(d\sigma_{22+}/d\omega_t)$, and short dashed line indicating $(2\pi/\sigma)(d\sigma_{21-}/d\omega_t)$. (d) Polar plots of $P(\theta_r,\phi_r)$ distribution averaged over all scattering angles.

TABLE 2: The Mean Values of Moduli of L, L′ and J′, Expressed in Units of $\hbar$

reactions		attractive	mixed	repulsive
L + HL	$\langle L \rangle$	3.63	2.97	2.56
	$\langle L' \rangle$	1.51	1.26	0.90
	$\langle J' \rangle$	3.34	2.92	2.52
L + LH	$\langle L \rangle$	6.37	5.86	5.37
	$\langle L' \rangle$	5.36	5.18	5.18
	$\langle J' \rangle$	2.12	2.01	2.67
L + HH	$\langle L \rangle$	5.09	3.65	3.29
	$\langle L' \rangle$	5.68	3.58	3.28
	$\langle J' \rangle$	4.07	2.28	1.83

From the results of $(2\pi/\sigma)(d\sigma_{00}/d\omega_t)$, one can conclude that the products are scattered strongly forward on attractive surface, but sideways scattering appears on mixed and repulsive surfaces. Obviously, $(2\pi/\sigma)(d\sigma_{00}/d\omega_t)$ is sensitive to character types of the surfaces. The behavior of $(2\pi/\sigma)(d\sigma_{20}/d\omega_t)$ shows strongly dependence on scattering angles on all three surfaces. On the attractive surface, the distribution of $(2\pi/\sigma)(d\sigma_{20}/d\omega_t)$ shows the trend which is opposite to that of $(2\pi/\sigma)(d\sigma_{00}/d\omega_t)$ indicating that $\mathbf{J}'$ strongly aligned perpendicular to $\mathbf{K}$. As we know, PDDCS $(2\pi/\sigma)(d\sigma_{20}/d\omega_t)$ is related to $P_2(\cos\theta r)$, and the expected value of $\langle P_2(\cos\theta_r)\rangle$ on the attractive surface is -0.34. As discussed above about the LHL mass combination, such behavior is easily understood from the eqs 6 and 7. It is noted that the PDDCS $(2\pi/\sigma)(d\sigma_{22+}/d\omega_t)$ is strongly polarized with scattering angle on all surfaces. $(2\pi/\sigma)(d\sigma_{21-}/d\omega_t)$, which shows anisotropic characteristics on mixed and repulsive surfaces, suggests that $\mathbf{J}'$ is not strongly aligned along with the y axis as $\mathbf{J}'$ of the LHL mass combination. In summary, $(2\pi/\sigma)(d\sigma_{00}/d\omega_t)$, $(2\pi/\sigma)(d\sigma_{20}/d\omega_t)$, $(2\pi/\sigma)(d\sigma_{22+}/d\omega_t)$, and $(2\pi/\sigma)(d\sigma_{21-}/d\omega_t)$ show a strong dependence on the characteristics of the surfaces. From the plots of $P(\theta_r,\phi_r)$, two peaks are shown on the attractive surface. But, only one strong peak is appears on the mixed and repulsive surfaces, which is in good agreement with the results of $P(\theta_r)$ and $P(\phi_r)$.

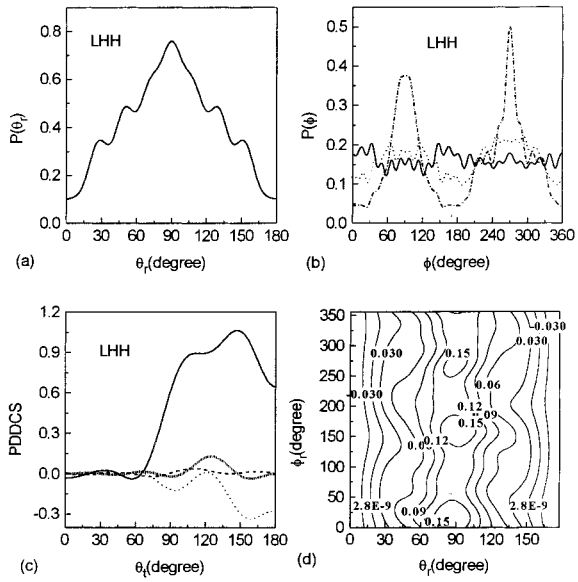

Figure 9. The results on attractive surface for the LHH mass combination. (a) The distribution of $P(\theta_r)$, reflecting the $\mathbf{K}-\mathbf{J}'$ correlation. (b) Solid line indicating the distribution $P(\phi_r)$, dotted line indicating $P(\phi_{L'})$, dot−dashed line indicating $P(\phi_L)$. (c) Four PDDCSs, solid line indicating $(2\pi/\sigma)(d\sigma_{00}/d\omega_t)$, dotted line indicating $(2\pi/\sigma)(d\sigma_{20}/d\omega_t)$, short vertical line indicating $(2\pi/\sigma)(d\sigma_{22+}/d\omega_t)$, and short dashed line indicating $(2\pi/\sigma)(d\sigma_{21-}/d\omega_t)$. (d) Polar plots of $P(\theta_r,\phi_r)$ distribution averaged over all scattering angles.

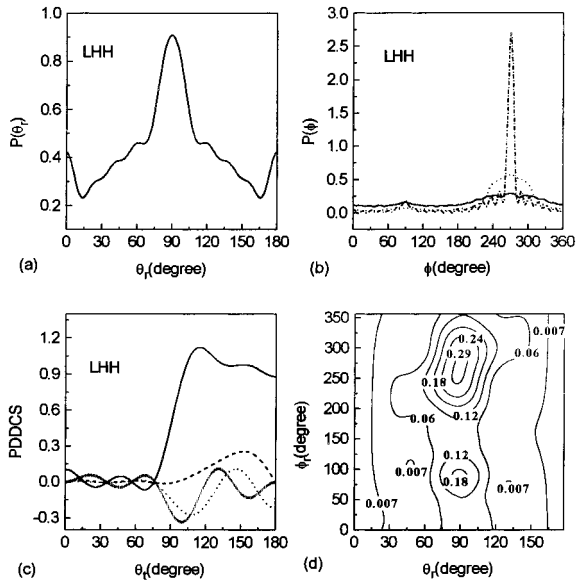

Figure 10. The results on mixed surface for the LHH mass combination. (a) The distribution of $P(\theta_r)$, reflecting the $\mathbf{K}-\mathbf{J}'$ correlation. (b) Solid line indicating the distribution $P(\phi_r)$, dotted line indicating $P(\phi_{L'})$, dot−dashed line indicating $P(\phi_L)$. (c) Four PDDCSs, solid line indicating $(2\pi/\sigma)(d\sigma_{00}/d\omega_t)$, dotted line indicating $(2\pi/\sigma)(d\sigma_{20}/d\omega_t)$, short vertical line indicating $(2\pi/\sigma)(d\sigma_{22+}/d\omega_t)$ and short dashed line indicating $(2\pi/\sigma)(d\sigma_{21-}/d\omega_t)$. (d) Polar plots of $P(\theta_r,\phi_r)$ distribution averaged over all scattering angles.

C. Light−Heavy−Heavy (LHH) Mass Combination. Figures 9−11 show the influences of surfaces on product angular polarization for the LHH mass combination. The effect of surfaces on the distribution of $P(\theta_r)$ is evident. Comparing the results with those of the LHL mass combination, one can conclude that the distribution of $P(\theta_r)$ is more broad than those of LHL mass combination on all three surfaces. Although $P(\theta_r)$ is influenced by surfaces, the weak product rotational alignments are shown on all three surfaces. In the case of the LHH mass

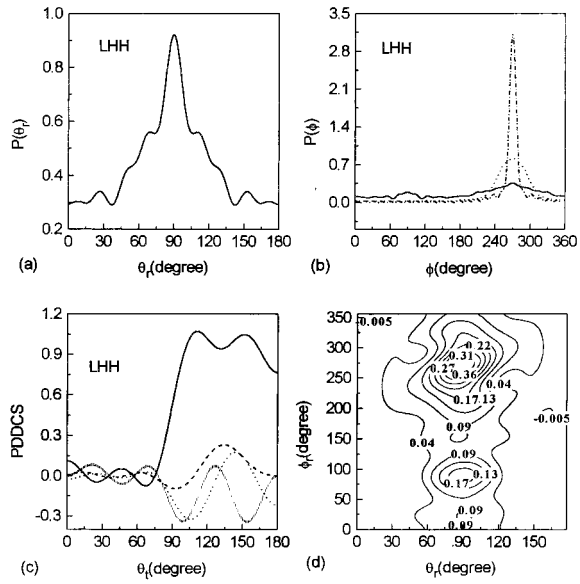

Figure 11. The results on repulsive surface for the LHH mass combination. (a) The distribution of $P(\theta_r)$, reflecting the $\mathbf{K}-\mathbf{J}'$ correlation. (b) Solid line indicating the distribution $P(\phi_r)$, dotted line indicating $P(\phi_{L'})$, dot−dashed line indicating $P(\phi_L)$. (c) Four PDDCSs, solid line indicating $(2\pi/\sigma)(d\sigma_{00}/d\omega_t)$, dotted line indicating $(2\pi/\sigma)(d\sigma_{20}/d\omega_t)$, short vertical line indicating $(2\pi/\sigma)(d\sigma_{22+}/d\omega_t)$, and short dashed line indicating $(2\pi/\sigma)(d\sigma_{21-}/d\omega_t)$. (d) Polar plots of $P(\theta_r,\phi_r)$ distribution averaged over all scattering angles.

combination, the product orbital angular momentum $\mathbf{L}'$ is large, and the reactant orbital angular momentum has less influence on the molecular product rotational alignment than that of the LHL mass combination.

From the dihedral angle distribution $P(\phi_r)$, one comes to a conclusion that $P(\phi_r)$ shows weak polarization on attractive surface. However, on mixed and repulsive surfaces, most of product molecules are scattered with $\phi_r \geq \pi$. Following the distributions of $P(\phi_{L'})$, $P(\phi_L)$, and $P(\phi_r)$ and mean values of $\mathbf{L}$, $\mathbf{L}'$, and $\mathbf{J}'$, the propensity $\mathbf{L} \rightarrow \mathbf{L}'$ is stronger on mixed and repulsive surfaces than that of attractive surface. As a result of $P(\phi_r)$ for LHL, LLH, and LHH mass combinations, the reaction with molecular product with $\phi_r \leq \pi$ proceeds more preferentially on the attractive surface than the reactions on mixed and repulsive surfaces, which are easily understood from the distribution of distributions of $P(\phi_{L'})$, $P(\phi_L)$, and $P(\phi_r)$ and mean values of $\mathbf{L}$, $\mathbf{L}'$, and $\mathbf{J}'$ in Table 2.

It is obvious that the surfaces have a weak influence on PDDCS $(2\pi/\sigma)(d\sigma_{00}/d\omega_t)$. On all three surfaces, the angular scattering tends to be backward scattering. The behavior of PDDCS $(2\pi/\sigma)(d\sigma_{20}/d\omega_t)$ shows anisotropic trend for backward scattering on all three surfaces. Clearly, $(2\pi/\sigma)(d\sigma_{20}/d\omega_t)$ is sensitive to characters of surfaces. On the attractive surface, the value of PDDCS $(2\pi/\sigma)(d\sigma_{22+}/d\omega_t)$ is positive at the scattering angle of 125°, which reveals that the product rotational angular momentum $\mathbf{J}'$ is aligned along the x axis, which is in good agreement with $P(\phi_r)$. The PDDCS $(2\pi/\sigma)(d\sigma_{21-}/d\omega_t)$, which shows strong anisotropy for backward scattering on mixed and repulsive surfaces, might indicate that $P(\theta_r)$ shows weak polarization and that $P(\phi_r)$ is aligned along the y axis to some degree. As the results of $(2\pi/\sigma)(d\sigma_{21-}/d\omega_t)$ indicate, one can conclude that $(2\pi/\sigma)(d\sigma_{21-}/d\omega_t)$ is polarized more weakly on the attractive surface than on the mixed and repulsive surfaces, which may result from the fact that the $P(\theta_r)$ is strongly polarized on the attractive surface than on the mixed and repulsive surfaces. Obviously, $(2\pi/\sigma)(d\sigma_{20}/d\omega_t)$, $(2\pi/\sigma)(d\sigma_{22+}/d\omega_t)$, and $(2\pi/\sigma)(d\sigma_{21-}/d\omega_t)$ are sensitive to surface type. From

the plots of $P(\theta_r,\phi_r)$, one notes that three weak peaks appear on attractive surface and that two peaks are shown on mixed and repulsive surfaces, which are in accordance with $P(\theta_r)$ and $P(\phi_r)$.

IV. Conclusions

This paper has presented a quasiclassical trajectory study of dependence of rotational angular momentum polarization for LHL, LLH, and LHH mass combination on the attractive, mixed, and repulsive surfaces at a collision energy of 10.0 kcal/mol. For the LHL mass combination, the mass combination plays a key role on $P(\theta_r)$, so that the distribution of $P(\theta_r)$ is almost independent on surfaces. For LLH and LHH mass combinations, $P(\theta_r)$ is sensitive to surfaces. Furthermore, it is concluded that the molecular products with $\phi < \pi$ are scattered much more on the attractive surface than those on the mixed and repulsive surfaces. In case of LHL mass combination, $(2\pi/\sigma)(d\sigma_{21-}/d\omega_t)$, $(2\pi/\sigma)(d\sigma_{00}/d\omega_t)$, $(2\pi/\sigma)(d\sigma_{20}/d\omega_t)$, and $(2\pi/\sigma)(d\sigma_{22+}/d\omega_t)$ are weakly affected by the surfaces. For the LLH mass combinations, $(2\pi/\sigma)(d\sigma_{00}/d\omega_t)$, $(2\pi/\sigma)(d\sigma_{20}/d\omega_t)$, $(2\pi/\sigma)(d\sigma_{22+}/d\omega_t)$, and $(2\pi/\sigma)(d\sigma_{21-}/d\omega_t)$ show a strong dependence on the characteristics of the surfaces. In case of LHH mass combination, the surfaces have a weak influence on $(2\pi/\sigma)(d\sigma_{00}/d\omega_t)$, however, $(2\pi/\sigma)(d\sigma_{20}/d\omega_t)$, $(2\pi/\sigma)(d\sigma_{22+}/d\omega_t)$, and $(2\pi/\sigma)(d\sigma_{21-}/d\omega_t)$ are sensitive to surface type. Finally, we hope that this calculation may provide us with some help, when we interpret their experimental data.

Acknowledgment. This work is supported in part by the National Science Foundation of China and the State Committee of Science and Technology of China.

References and Notes

(1) Simons, J. P. *J. Phys. Chem*. **1987**, *91*, 5378.
(2) Fano, U.; Macek, J. H. *Rev. Mod. Phys*. **1973**, *45*, 553.
(3) Case, D. E.; Herschbach, D. R. *Mol. Phys*. **1975**, *30*, 1537.
(4) Mcclelland, G. M.; Herschbach, D. R. *J. Phys. Chem*. **1979**, *83*, 1445.
(5) Barnwell, J. D.; Loeser, J. G.; Herschbach, D. R. *J. Phys. Chem*. **1983**, *87*, 2781.
(6) Aoiz, F. J.; Brouard, M.; Enriquez, P. A. *J. Chem. Phys*. **1996**, *105*, 4964.
(7) Jonah, C. D.; Zare, R. N.; Ottinger, C. *J. Chem. Phys*. **1972**, *56*, 2631.
(8) Engelke, F.; Meiwes-broer, K. H. *Chem. Phys. Lett*. **1984**, *108*, 132.
(9) Li, R. J.; Li, F.; Han, K. L.; Lu, R. C.; He, G. Z.; Lou, N. Q. *Chem. Phys. Lett*. **1994**, *220*, 281.
(10) Hsu, D. S. Y.; Weinstein, N. D.; Herschbach, D. R. *Mol. Phys*. **1975**, *29*, 257.
(11) Wang, M. L.; Han, K. L.; Zhan, J. P.; Wu, W. V. K.; He, G. Z.; Lou, N. Q. *Chem. Phys. Lett*. **1997**, *278*, 307.
(12) Zhan, J. P.; Yang, H. P.; Han, K. L.; Deng, W. Q.; He, G. Z.; Lou, N. Q. *J. Phys. Chem. A*. **1997**, *101*, 7486.
(13) Ding, G. W.; Sun, W. Z.; Yang, W. S.; Xu, D. L.; Zhao, R. P.; He, G. Z.; Lou, N. Q. *Chem. Phys. Lett*. **1997**, *265*, 392.
(14) Orr-Ewing, A. J.; Zare, R. N. *Annu. Rev. Phys. Chem.* **1994**, *45*, 315.
(15) Orr-Ewing, A. J.; Zare, R. N. In *Chemical Dynamics and Kinetics of Small Free Radicals*; Wagner, A., Liu, K., Eds.; World Scientific: Singapore, 1995; p 936.
(16) Brouard, M.; Simons, J. P. In *Chemical Dynamics and Kinetics of Small Free Radicals*; Wagner, A., Liu, K., Eds.; World Scientific: Singapore, 1995; p 795.
(17) Kim, L.; Wickramaaratchi, M. A.; Hall, G. E. *J. Chem. Phys*. **1994**, *101*, 2033.
(18) Brouard, M.; Duxon, S.; Enriquez, P. A.; Simons, J. P. *J. Chem. Soc., Faraday Trans*. **1993**, *89*, 1432.
(19) Brouard, M.; Lambert, H. M.; Short, J.; Simons, J. P. *J. Phys. Chem.* **1995,** *99*, 13571.
(20) Orr-Ewing, A. J.; Simpon, W. R.; Rakitzis, T.P.; Kandel. S. A.; Zare, R. N. *J. Chem. Phys.* **1997**, *106*, 5961.
(21) Rakitzis, T. P.; Kandel. S. A.; Lev-On, T.; Zare, R. N, *J. Chem. Phys.* **1997**, *107*, 9392.
(22) Polanyi, J. C.; Wong, W. H. *J. Chem. Phys*. **1969**, *15*, 1439.
(23) Hijazi, N. H.; Polanyi, J. C. *Chem. Phys.* **1975**, *11*, 1.
(24) Hijazi, N. H.; Polanyi, J. C. *J. Chem. Phys*. **1975**, *63*, 2249.
(25) Han, K. L.; He, G. Z.; Lou, N. Q. *J. Chem. Phys*. **1996**, *105*, 8699.
(26) Ben-Nun, M.; Martinez, T. J.; Levine, R. D. *J. Phys. Chem. A* **1997**, *101*, 7522.
(27) Anderson, R. W. *J. Phys. Chem. A* **1997**, *101*, 7664.
(28) Brouard, M.; Lambert, H. M.; Rayner, S. P.; Simons, J. P. *Mol. Phys.* **1996**, *89*, 403.
(29) Aoiz, F. J.; Brouard, M.; Herrero, V. J.; Saez Rabanos, V.; Stark, K. *Chem. Phys. Lett.* **1997**, *264*, 487.
(30) Alexander, A. J.; Aoiz, F. J.; Banares, L.; Brouard, M.; Short, J.; Simons, J. P. *J. Phys. Chem. A* **1997**, *101*, 7544.
(31) Levine, R. D.; Bernstein, R. B. *Molecular Reaction Dynamics*; Oxford University Press: New York, 1974.
(32) Wang, M. L.; Han, K. L.; He, G. Z.; Lou, N. Q. *Ber. Bunsen-Ges. Phys. Chem*. **1997**, *101*, 1527.
(33) Kuntz, P. J.; Nemeth, E. M.; Polanyi, J. C.; Rosner, S. D.; Young, C. E. *J. Chem. Phys*. **1966**, *44*, 1168.
(34) Shafer-Ray, N. E.; Orr-Ewing, A. J.; Zare, R. N. *J. Phys. Chem*. **1995**, *99*, 7591.
(35) Wang, X. B.; Ben-Nun, M.; Levine, R. D. *Chem. Phys.* **1995**, *197*, 1.
(36) Wang, M. L.; Ham, K. L.; He, G. Z. *J. Chem. Phys.* **1998**, *109*, 5446.